Arborescent Amphiphilic Copolymers as Templates for the Preparation of Gold Nanoparticles

Jason Dockendorff,[†] Mario Gauthier,*[,†] Ahmed Mourran,[‡] and Martin Möller[‡]

Department of Chemistry, Institute for Polymer Research, University of Waterloo, 200 University Ave. W., Waterloo, Ontario N2L 3G1, Canada, and DWI an der RWTH Aachen e.V. and Institute of Technical and Macromolecular Chemistry, RWTH Aachen, Pauwelsstrasse 8, D-52056 Aachen, Germany

Received June 11, 2008
Revised Manuscript Received August 12, 2008

Nanoparticle research has received much attention in recent years due to the unique properties and applications of these species. Metallic nanoparticles, in particular, have diverse application areas including imaging agents, nonlinear optics, microelectronics, separation science, diagnosis, targeted biological labeling and delivery systems, cell therapy or destruction, and catalysis.[1] Various methods have been examined for the preparation of metallic nanoparticles using polymeric templates. This includes self-assembled block copolymer reverse micelles[2a−c] and networks of amphiphilic polymers.[2d] The use of dendrimers and hyperbranched polymers as unimolecular scaffolds has also been successfully demonstrated.[3] We have investigated a new method for the preparation of metallic nanoparticles using a class of amphiphilic graft copolymers with a dendritic architecture, the arborescent polymers, as templates. Specifically, arborescent polystyrene-*graft*-[poly(2-vinylpyridine)-*block*-polystyrene] copolymers were applied to the preparation of gold nanoparticles. To this end, linear and branched polystyrene (PS) substrates were functionalized with acetyl coupling sites and grafted with "living" polystyrene-*block*-poly(2-vinylpyridine) chains. The resulting dendritic species have a covalently bonded, layered structure with an inner poly(2-vinylpyridine) (P2VP) shell that can be loaded with metallic salts or acids such as tetrachloroauric acid ($HAuCl_4$). The research to date has focused on $HAuCl_4$ because it is a well-documented nanoparticle precursor and is easily loaded within the P2VP phase. This system is compatible with different reduction methods, but we investigated solution reduction using hydrazine (N_2H_4) so far.

The unimolecular micelle architecture is a much more stable template for loading polar compounds than micelles formed by linear block copolymers, as it has no critical micelle concentration. Aside from their inherent stability, arborescent polymer templates have the potential to offer other important advantages over established methods. For example, variation in the degree of polymerization of the side chain building blocks and the number of grafting cycles (generation) provides control over the characteristics of the templates (e.g., core size, chain mobility, stabilizing layer thickness) beyond what is achievable by the self-assembly of block copolymer chains. These characteristics may be important to tailor the activity of these nanospecies in catalytic applications[4] or their optical properties relevant to biological applications such as cell therapy.[1a,e−g] This Communication focuses on preliminary results obtained with G0 [PS-*g*-(P2VP-*b*-PS)] and G2 [G1PS-*g*-(P2VP-*b*-PS)] arborescent copolymer templates loaded with $HAuCl_4$ at various levels and subsequently reduced in solution with hydrazine. A schematic representation of the grafting reaction and loading procedure is provided in Figure 1, while detailed synthetic procedures and characterization data for the templates can be found in the Supporting Information.

The grafting reaction was carried out under conditions previously reported by our group;[5] however, it was determined that the inherent characteristics of the PS-*b*-P2VP side chains make the outcome of the grafting reaction less favorable. We believe that the grafting yield for these reactions is unexpectedly low due to the ability of the living PS-*b*-P2VP$^-$ chains to assemble into micellar structures. Diffusion of the P2VP living centers to the coupling sites on the substrate would be hindered if micelles are formed, consequently reducing the grafting yield (defined as the fraction of the side chains generated becoming attached to the substrate). The grafting yield attained for the G0 and G2 templates used in the current investigation was 17% and 20%, respectively. This contrasts with the grafting yields previously reported for G0 and G2 species with side chains of comparable dimensions, namely 87% and 55% for PS homopolymers[6] and 86% and 34% for copolymers obtained by grafting P2VP chains onto PS substrates.[5]

Prior to the dendritic templates, reverse micelles derived from the self-assembly of linear PS-*b*-P2VP copolymers were loaded with $HAuCl_4$ to ensure that our loading procedure replicated published results.[7] Initial loading attempts for arborescent copolymer molecules with short polystyrene segments in the corona (number-average degree of polymerization $DP_n = 66$) led to extensive aggregation of the metal-loaded templates. This was attributed to the inability of short polystyrene segments to shield the interactions of the charged, metal-loaded P2VP shell of the arborescent copolymers. Aggregation could be reduced to some extent by loading the templates in a polar solvent such as tetrahydrofuran, but this would likely reduce the loading level attained because of the high solubility of $HAuCl_4$ in polar solvents. Better results were obtained for templates incorporating longer PS segments in the corona. The DP_n of the polystyrene segments in the G0 and G2 templates reported herein was 108 and 192, respectively. The longer PS chains of these templates were able to shield interactions between charged cores and thus hindered aggregation more effectively.

Variations in the loading level revealed that higher loadings led to increased intertemplate separation and a more uniform dispersion of the templates within films cast from the solutions. The size of the gold salt-loaded domains within the templates did not appear to depend on the loading level. The average diameter of these domains was quite different for the two template generations investigated as expected, however, being

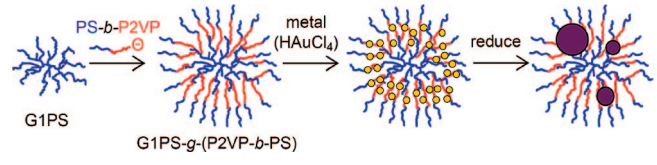

Figure 1. Schematic representation of the arborescent (G2) copolymer template synthesis, metallic salt loading, and reduction.

* To whom correspondence should be addressed. E-mail: gauthier@uwaterloo.ca.
[†] University of Waterloo.
[‡] RWTH Aachen.

10.1021/ma801320r CCC: $40.75
Published on Web 08/21/2008

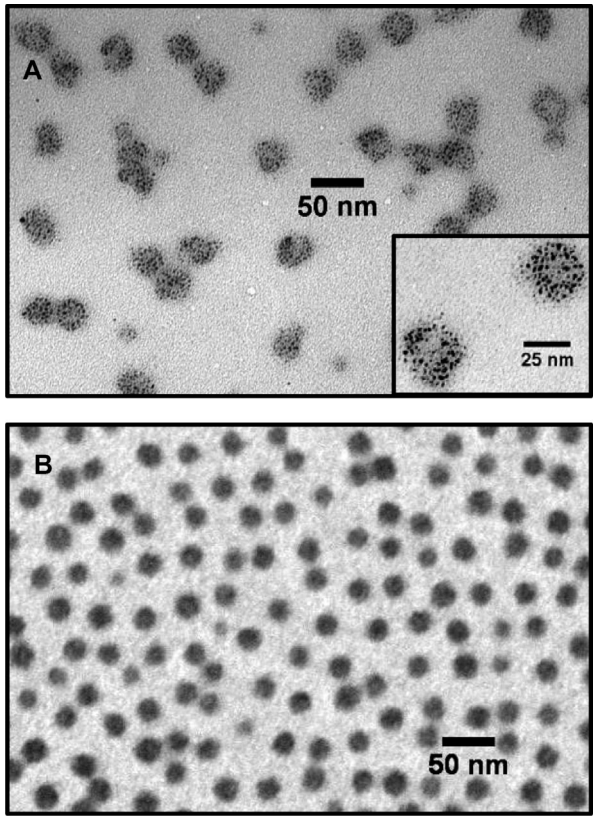

Figure 2. Example of TEM micrographs obtained for G2 (A) and G0 (B) templates loaded with $HAuCl_4$ at 0.25 and 0.50 equiv relative to 2VP residues, respectively.

19 ± 2 and 30 ± 3 nm for the G0 and G2 templates, respectively.

Comparison of the upper (G2) and lower generation (G0) templates is interesting, since higher generation polymers have a larger PS core and a core−shell morphology that is better developed.[8] A nonuniform distribution of gold salt within the G2 templates was indeed observed in some cases, the periphery being more densely loaded than the center, as seen in Figure 2A. This quasi-ring-like organization of the metal within the P2VP shell of the G2 templates is indicative of the layered morphology of the molecules and could potentially open the way to the preparation of "hollow" metallic nanoparticles. The G0 templates, in contrast, were characterized by a homogeneous distribution of gold salt in the center of the micelles (Figure 2B) due to the small and ill-defined hydrophobic core comprised of a single polystyrene chain. The results for the G0 template are similar to gold-loaded block copolymer micelles[2a] since these have a fully loadable interior. The better defined, larger G1 PS core within the G2 template at the center of the structure would necessarily lead to more important contrast variations in the TEM measurements.

It is understood that the gold salt contained within the template molecules shown in Figure 2 is reduced to elemental gold by the electron beam in the TEM measurements.[7] Solution reduction of the templates is obviously more convenient for the production of gold nanoparticles on a large scale, however. Consequently, solution reduction of the nanoparticles with hydrazine was examined in two different regimes, namely near equivalence and excess stoichiometry. The excess regime (10:1, N_2H_4:Au) led to the collapse of the very small (<1 nm) gold salt clusters into one or multiple larger, somewhat narrowly dispersed solid particles within each template. This is shown

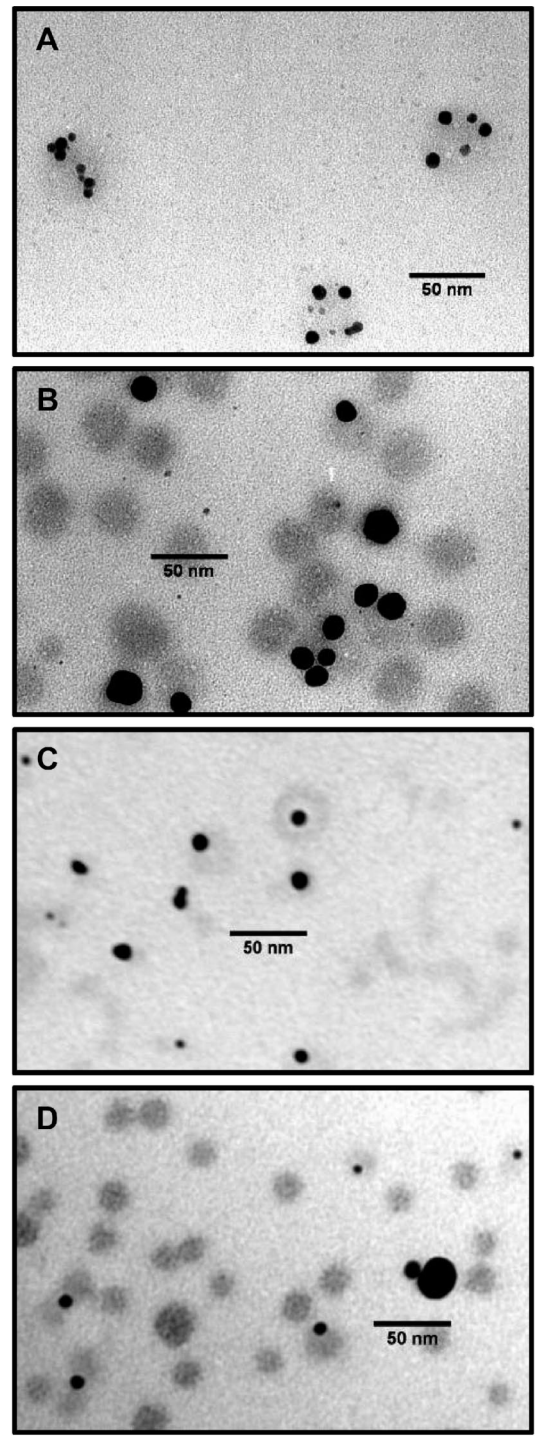

Figure 3. Reduced gold nanoparticles obtained from the G2 template (A, 10:1 N_2H_4:Au; B, 1.2:1 N_2H_4:Au) and the G0 template (C, 10:1 N_2H_4:Au; D, 1.2:1 N_2H_4:Au).

in Figures 3A,C. The size and size distribution of the collapsed nanoparticles remained consistent across all loading levels for each template within this regime. Surprisingly, the size of the gold nanoparticles obtained under these conditions from the G0 and G2 templates was essentially identical within error limits, being 10 ± 3 and 8 ± 3 nm, respectively.

Solution reduction in the near-equivalency regime (1.2:1, N_2H_4:Au) also induced collapse of the gold particles into solid nanoparticles; however, the aggregation of these nanoparticles was more obvious since a larger average size and a broader size distribution were observed. This phenomenon is illustrated in Figures 3B,D. In analogy to the excess regime and the

Table 1. Size Analysis from TEM Micrographs of Gold-Loaded Templates

sample	reduction (N_2H_4:Au)	feature[a]	diameter (nm) at loading level[b] 0.125 equiv	0.25 equiv	0.50 equiv	1.00 equiv
G2 + Au	none		31 ± 2	30 ± 3	30 ± 3	28 ± 2
G2 + Au	10:1	solid	8 ± 2	8 ± 2	8 ± 2	9 ± 3
G2 + Au	1.2:1	solid	13 ± 3	15 ± 5	17 ± 9	15 ± 7
G2 + Au	1.2:1	shadow	31 ± 3	30 ± 3		30 ± 2
G0 + Au	none		20 ± 2	22 ± 2	20 ± 3	20 ± 3
G0 + Au	10:1	solid	9 ± 2	10 ± 3	10 ± 3	11 ± 3
G0 + Au	1.2:1	solid	20 ± 8	12 ± 4	10 ± 6	21 ± 2
G0 + Au	1.2:1	shadow	18 ± 2	18 ± 2	18 ± 2	20 ± 2

[a] Refers to the feature dimensions when more than one feature present; solid (black), shadow (gray) as seen in Figure 3. [b] Equivalents of $HAuCl_4$ relative to 2VP units.

nonreduced systems, the size and size distribution of the nanoparticles were insensitive to the loading level. These results for the reduction reaction are consistent with those of Chiang for gold nanoparticles constructed within surfactant reverse micelles,[9] who reported larger and less uniform gold particles when the molar ratio of hydrazine to $HAuCl_4$ was decreased. It should be noted that in the near-equivalency regime apparently less than 100% of the gold collapsed into solid nanoparticles: a faint shadow of the same size as the nonreduced particles remained in the background. Detailed size information extracted from TEM micrograph analysis can be found in Table 1.

In summary, it was found that the characteristics of the arborescent PS-*g*-(P2VP-*b*-PS) copolymer templates govern the distribution of the gold salt loaded within the molecules. Templates containing large, better defined hydrophobic cores such as G1PS-*g*-(P2VP-*b*-PS) appear to have lighter salt loading near the center of the molecule, while smaller G0 templates such as PS-*g*-(P2VP-*b*-PS) are characterized by uniform loading within the core. The solution reduction studies revealed that the size and uniformity of the gold nanoparticles obtained were independent of template generation and rather reliant on the amount of reducing agent used. Excess reducing agent prevented aggregation and led to a more uniform size distribution of the gold nanoparticles.

Ongoing research includes an investigation of the influence of the P2VP chain length in the molecules as well comparisons for a full range of template generations (G0−G4). It is expected that higher generation templates will have a more distinct core and a better defined ring structure.

Acknowledgment. We gratefully thank the Natural Sciences and Engineering Research Council of Canada (NSERC), the German Academic Exchange Service (DAAD), and Mr. Dale Weber (TEM) for their support of the work.

Supporting Information Available: Background information, experimental details (including synthesis, sample preparation, and instrumentation), and characterization data. This material is available free of charge via the Internet at http://pubs.acs.org.

References and Notes

(1) (a) Jain, P. K.; Huang, X.; El-Sayed, I. H.; El-Sayed, M. A. *Plasmonics* **2007**, *2*, 107–118. (b) Tsuchiya, K.; Nagayasu, S.; Okamoto, S.; Hayakawa, T.; Hihara, T.; Yamamoto, K.; Takumi, I.; Hara, S.; Hasegawa, H.; Akasaka, S.; Kosikawa, N. *Opt. Express* **2008**, *16*, 5362–5371. (c) Garnett, E. C.; Liang, W.; Yang, P. *Adv. Mater.* **2007**, *19*, 2946–2950. (d) Nilsson, C.; Birnbaum, S.; Nilsson, S. *J. Chromatogr. A* **2007**, *1168*, 212–224. (e) Qian, X.-M.; Nie, S. M. *Chem. Soc. Rev.* **2008**, *37*, 912–920. (f) Azarmi, S.; Roa, W. H.; Löbenberg, R. *Adv. Drug Delivery Rev.* **2008**, *60*, 863–875. (g) Podsiadlo, P.; Sinani, V. A.; Bahng, J. H.; Kam, N. W. S.; Lee, J.; Kotov, N. A. *Langmuir* **2008**, *24*, 568–574. (h) Gannon, C. J.; Patra, C. R.; Bhattacharya, R.; Mukherjee, P.; Curley, S. A. *J. Nanobiotechnol.* **2008**, *6*, 2. (i) Xu, C.; Sun, S. *Polym. Int.* **2007**, *56*, 821–826. (j) Bhattacharya, R.; Patra, C. R.; Earl, A.; Wang, S.; Katarya, A.; Lu, L.; Kizhakkedathu, J. N.; Yaszemski, M. J.; Greipp, P. R.; Mukhopadhyay, D.; Mukherjee, P. *Nanomed. Nanotechnol. Biol. Med.* **2007**, *3*, 224–238. (k) Schimpf, S.; Lucas, M.; Mohr, C.; Rodemerck, U.; Brückner, A.; Radnik, J.; Hofmeister, H.; Claus, P. *Catal. Today* **2002**, *72*, 63–78.

(2) See for example: (a) Spatz, J. P.; Sheiko, S.; Möller, M. *Macromolecules* **1996**, *29*, 3220–3226. (b) Filali, M.; Meier, M. A. R.; Schubert, U. S.; Gohy, J.-F. *Langmuir* **2005**, *21*, 7995–8000. (c) Koh, H.-D.; Kang, N.-G.; Lee, J.-S. *Langmuir* **2007**, *23*, 11425–11429. (d) Hansen, C. R.; Westerlund, F.; Moth-Poulsen, K.; Ravindranath, R.; Valiyaveettil, S.; Bjørnholm, T. *Langmuir* **2008**, *24*, 3905–3910.

(3) See for example: (a) Zhao, M.; Sun, L.; Crooks, R. M. *J. Am. Chem. Soc.* **1998**, *120*, 4877–4878. (b) Balogh, L.; Tomalia, D. A. *J. Am. Chem. Soc.* **1998**, *120*, 7355–7356. (c) Balogh, L.; deLeuze-Jallouli, A. M.; Dvornic, P. R.; Owen, M. J.; Perz, S. V.; Spindler, R. U.S. Patent 5938934, **1999**. (d) Gröhn, F.; Bauer, B. J.; Akpalu, Y. A.; Jackson, C. L.; Amis, E. J. *Macromolecules* **2000**, *33*, 6042–6050. (e) Dvornic, P. R.; Hu, J.; Reeves, S. D.; Owen, M. J. *Silicon Chem.* **2002**, *1*, 177–193. (f) Seo, Y.-S.; Kim, K.-S.; Shin, K.; White, H.; Rafailovich, M.; Sokolov, J.; Lin, B.; Zhang, C.; Balogh, L. *Langmuir* **2002**, *18*, 5927–5932. (g) Dvornic, P. R.; Bubeck, R. A.; Reeves, S. D.; Li, J.; Hoffman, L. W. *Silicon Chem.* **2003**, *2*, 207–216. (h) Bubeck, R. A.; Dvornic, P. R.; Hu, J.; Hexemer, A.; Li, X.; Keinath, S. E.; Fischer, D. A. *Macromol. Chem. Phys.* **2005**, *206*, 1146–1153. (i) Wan, D.; Fu, Q.; Huang, J. *J. Appl. Polym. Sci.* **2006**, *101*, 509–514. (j) Zhang, J.; Meng, L.; Zhao, D.; Fei, Z.; Lu, Q.; Dyson, P. J. *Langmuir* **2008**, *24*, 2699–2704.

(4) Klingelhöfer, S.; Heitz, W.; Grenier, A.; Oestreich, S.; Förster, S.; Antonietti, M. *J. Am. Chem. Soc.* **1997**, *119*, 10116–10120.

(5) Gauthier, M.; Li, J.; Dockendorff, J. *Macromolecules* **2003**, *36*, 2642–2648.

(6) Li, J.; Gauthier, M. *Macromolecules* **2001**, *34*, 8918–8924.

(7) Mössmer, S.; Spatz, J. P.; Möller, M.; Aberle, T.; Schmidt, J.; Burchard, W. *Macromolecules* **2000**, *33*, 4791–4798.

(8) Yun, S. I.; Lai, K.; Briber, R. M.; Teertstra, S. J.; Gauthier, M.; Bauer, B. J. *Macromolecules* **2008**, *41*, 175–183.

(9) Chiang, C. *J. Colloid Interface Sci.* **2001**, *239*, 334–341.

MA801320R